OrBITS: A High-throughput, time-lapse, and label-free drug screening platform for patient-derived 3D organoids

Authors: Christophe Deben[1*], Edgar Cardenas De La Hoz[2]*, Maxim Le Compte[1], Paul Van Schil[3], Jeroen M. Hendriks[3], Patrick Lauwers[3], Suresh Krishan Yogeswaran[3], Filip Lardon[1], Patrick Pauwels[1,4], Annemie Bogaerts[6], Evelien Smits[1,5], Steve Vanlanduit[2], Abraham Lin[1,6]

*Both authors contributed equally to the manuscript. Christophe Deben for the biological part, Edgar Cardenas De La Hoz for the computational part.

1. Center for Oncological Research (CORE), Integrated Personalized & Precision Oncology Network (IPPON), University of Antwerp, Wilrijk, Belgium.

2. Industrial Vision Lab, University of Antwerp, Groenenborgerlaan 171, Antwerp 2020, Belgium

3. Department of Thoracic and Vascular surgery, Antwerp University Hospital, Edegem, Belgium.

4. Department of Pathology, Antwerp University Hospital, Edegem, Belgium.

5. Center for Cell Therapy and Regenerative Medicine, Antwerp University Hospital, Edegem, Belgium.

6. Plasma Lab for Applications in Sustainability and Medicine ANTwerp (PLASMANT), University of Antwerp, 2610 Wilrijk, Belgium.

Abstract

Patient-derived organoids are invaluable for fundamental and translational cancer research and holds great promise for personalized medicine. However, the shortage of available analysis methods, which are often single-time point, severely impede the potential and routine use of organoids for basic research, clinical practise, and pharmaceutical and industrial applications. Here, we report the development of a high-throughput automated organoid analysis platform that allows for kinetic monitoring of organoids, named **Or**ganoid **B**rightfield **I**dentification-based **T**herapy **S**creening (OrBITS). The combination of computer vision with a convolutional network machine learning approach allowed for the detection and tracking of organoids in routine extracellular matrix domes, advanced Gri3D®-96 well plates, and high-throughput 384-well microplates, solely based on brightfield imaging. We used OrBITS to screen chemotherapeutics and targeted therapies, and incorporation of a fluorescent cell death marker, revealed further insight into the mechanistic action of the drug, a feature not achievable with the current gold standard ATP-assay. This manuscript describes the validation of the OrBITS deep learning analysis approach against current standard assays for kinetic imaging and automated analysis of organoids. OrBITS, as a scalable, high-throughput technology, would facilitate the use of patient-derived organoids for drug development, therapy screening, and guided clinical decisions for personalized medicine. The developed platform also provides a launching point for further brightfield-based assay development to be used for fundamental research.

Introduction

The use of 2D cancer cell lines has traditionally been the gold standard in preclinical *in vitro* cancer research. However, these models fail to recreate the complex cell-cell interactions present in the tumor microenvironment and lack the genetic heterogeneity found in cancer patients. In addition, prolonged use of these cancer cell lines lead to acquired mutations or gene expression alterations, which are often overlooked as the cell line deviates from the originally derived tumor. As a result, new therapies are often met with high failure rates during translation from preclinical research to clinical trials, thus resulting in extreme forfeiture of research labor and financial loss.

The development of 3D cell culture technologies has greatly improved the physiological relevance of *in vitro* cancer models and the use of patient-derived organoids (PDOs) is revolutionizing basic and translation cancer research [1]. These PDOs resemble both the pheno- and genotype of the tissue they are derived from and can be expanded long-term and cryopreserved to establish a living tumor and healthy tissue biobank [1]. Furthermore, one of the most promising applications of PDOs is for personalized cancer treatment to predict clinical response *ex vivo* [2-8]. However, the available repertoire of assays for high-throughput organoid analysis is severely limited, and therefore, the current gold standard relies on a rudimentary viability assay.

The gold standard analysis method, Promega CellTiter-Glo 3D cell viability assay, determines the number of viable cells in 3D cell cultures based on luminescent quantification of intracellular ATP in both 96- and 384-well microplate format. This is method is met with several intrinsic limitations including growth rate variations and (drug-induced) metabolic modulations, which could affect the translatability of this readout. [9-11] For drug screening and diagnostic applications, this assay is also unable to determine the mechanistic action of the drug, such as cytostatic or cytotoxic

response, and is limited to a single time-point analysis. These aspects critically limit the wide adoption of organoid technology for clinical diagnostics and pharmaceutical drug screening. Therefore, although the CellTiter-Glo viability assay has been a valuable method to monitor drug responses, more sophisticated high-throughput analysis methods are urgently needed.

In this study, we addressed these shortcomings by using an automated, high-throughput, and kinetic screening platform to monitor therapy response. Using the Tecan Spark Cyto multi-mode plate reader system, we automated seeding of full-grown PDOs in a 384-well format and performed real-time, whole-well brightfield (BF) and fluorescence imaging in a temperature, CO_2, and O_2 controlled environment. This reduces the variability involved in manual organoid cultures, which is highly cumbersome and not scalable. Using software, which utilizes convolutional network machine learning to eliminate the use of fluorescent viability markers, we validated the capacity for BF imaging-based monitoring of PDO growth and viability, by comparing our results to the current industry and research standards. The combination of BF imaging with a fluorescent cell death marker further demarcated cytostatic from cytotoxic therapy responses, thus providing greater insight into drug effects and the potential for improving translation into a durable clinical response in patients. The combination of the automated seeding and image-based monitoring of PDOs constitutes our novel integrated platform OrBITS (**Or**ganoid **B**rightfield **I**dentification-based **T**herapy **S**creening). Using OrBITS, we performed a screening of several chemotherapeutics and targeted therapies on patient-derived organoids as a proof-of-concept. The technology described here to produce and validate our drug screening platform unlocks the potential for wide adoption of organoid-based assays for drug screening and discovery as well as guidance of clinical decision for personalized medicine.

Results

Patient-derived lung organoids

Validation of the organoid monitoring ability using BF imaging was performed on various lung organoid lines. Organoids derived from patient tumor resection fragments had a predominantly solid growth pattern, while organoids derived from distant healthy lung tissue displayed a cystic growth pattern (Fig. S1). Further characterization of the tumor tissue-derived organoids indicated that the cells were non-malignant and most likely represent metaplastic squamous epithelial cells (details in supplementary information) [12,13]. These observations confirmed the challenges related to generating pure lung tumor organoids as first described by Dijkstra and colleagues. [13] However, for validation of organoid monitoring with OrBITS, these non-malignant organoids were equally relevant. The cystic NSCLC_006N and NSCLC_051N organoids and solid NSCLC_013T, NSCLC_046T and NSCLC_051T organoids were used in the subsequent experiments.

Validation of label-free Brightfield monitoring of all stages of organoid growth

A kinetic image set was generated from a serial dilution of single cells and 3-day old organoids grown in a 384-well microplate from two organoid lines (NSCLC_013T and NSCLC_006N) stained with Hoechst as a gold standard reference method. Pairwise comparison showed a strong correlation of the organoid Count, Mean Area, and Total Area detected by BF when compared to Hoechst for the entire range of sizes (Fig. 1A). This indicates that OrBITS is capable of kinetic monitoring at all stages of organoid growth in the absence of a fluorescent dye and based solely on BF image analysis (Fig. 1B, Supplemental Video 1-3).

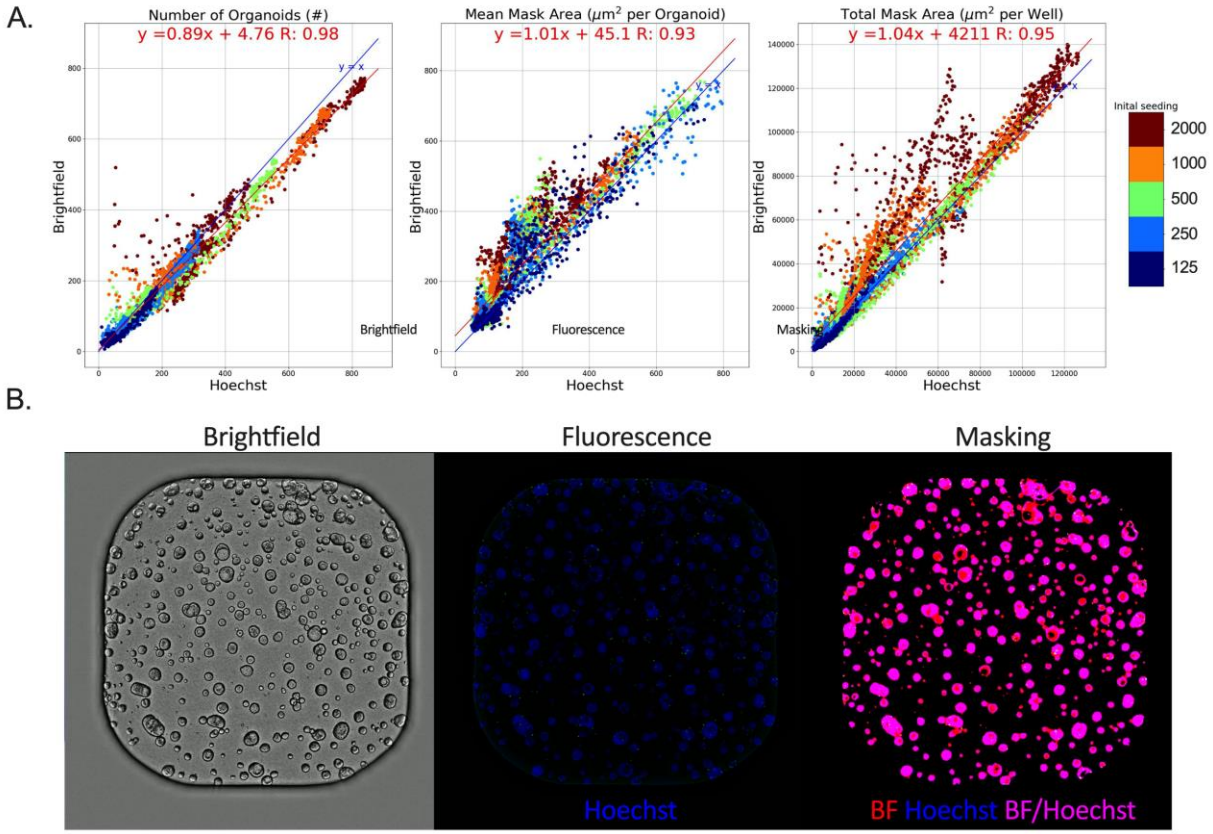

Figure 1: Brightfield versus Hoechst. (A) Pairwise comparison of organoid Counts, Mean Mask Area and Total Mask Area detected by Brightfield- and Hoechst-based analysis of NSCLC_013T and NSCLC_006N PDO lines plated as a serial dilution of single cells and 3-day old organoids (Table S2). (B) Representative whole 384-well brightfield and fluorescent images of full-grown PDOs and the corresponding analysis mask. Supplemental Video 3 presents the corresponding time-laps video.

Both organoid lines could be grown from either single cells (Fig. 2A) or fully-grown organoids, which are more conventionally used (Fig. 2B). An important advantage of the proposed assay is that growth kinetics can be accurately monitored using only a limited amount of starting material. In fact, using a larger number of single cells or organoids affected BF image monitoring results in two ways: (i) when both lines (NSCLC_013T and NSCLC_006N) were plated at high single cell densities, a drop in counts was observed over time due to organoids merging or fusion events (Fig.

125 2C-D, Supplemental Video 1) resulting in an aberrant growth rate based on Mean Area for
126 NSCLC_013T at higher seeding densities (Fig. 2A); (ii) NSCLC_006N PDOs showed a higher
127 growth rate compared to NSCLC_013T PDOs due to differential nutrient requirements. At higher
128 concentrations (>500 counts), we clearly observed a drop in NSCLC_006N organoids growth rate
129 compared to the slower growing NSCLC_013T organoids due to the lack of nutrients (Fig. 2B).

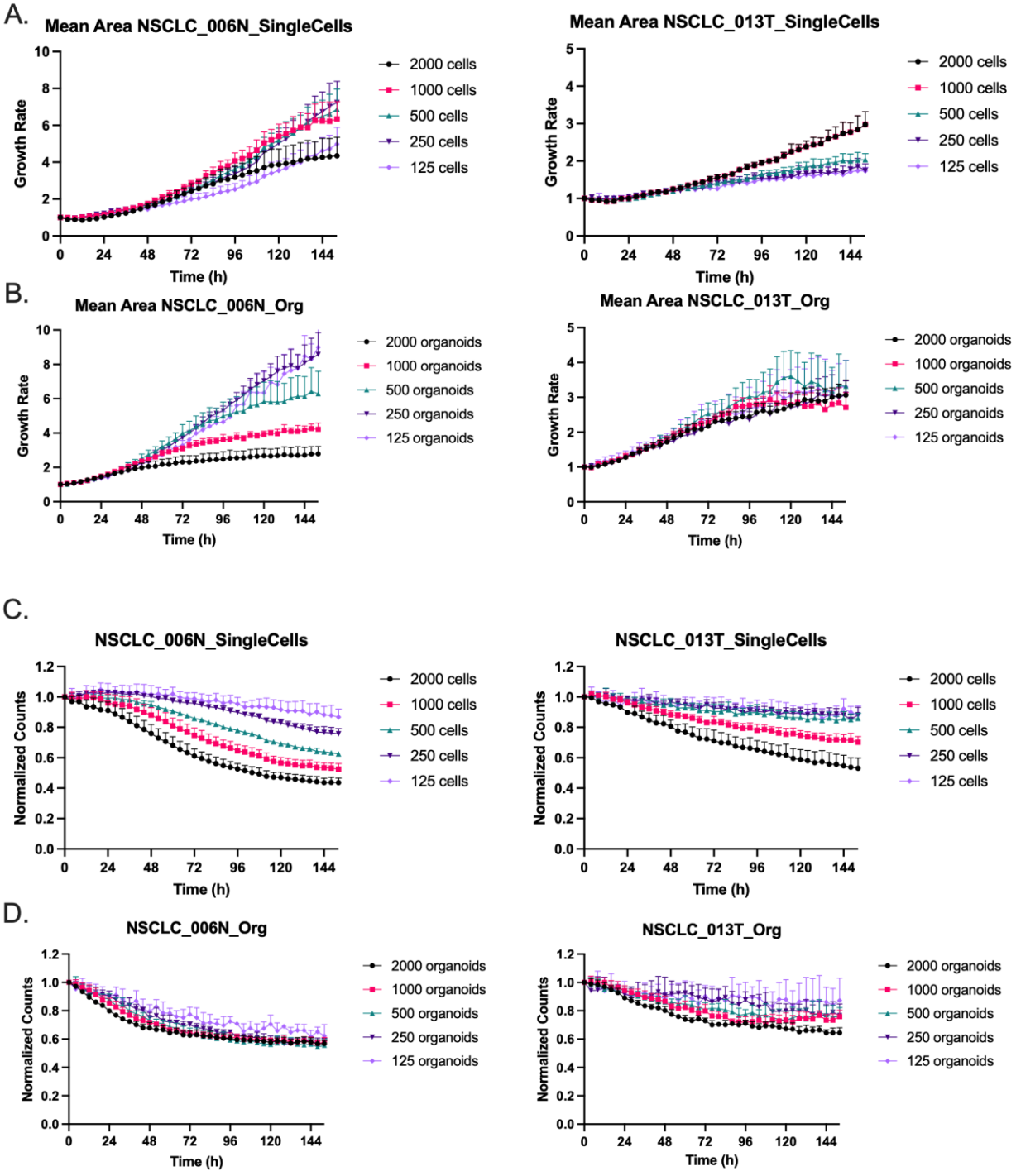

Figure 2: Influence of seeding density. Average growth rate of PDOs seeded as (A) single cells or (B) 3-day old organoids. Normalized counts (h=0) of PDOs seeded as (C) single cells or (D) 3-day old organoids. A range between 125 – 2000 cells or organoids were plated. Graphs presented as mean ± SD of 5 technical replicates and images were acquired every 6 hours.

Monitoring organoid death with intra-well normalization

Since PDOs used in drug screening will undergo varying degrees and stages of death, it is critical that the OrBITS platform is able to detect such organoids. Therefore, a second kinetic image set was generated from two organoid lines (NSCLC_051T and NSCLC_051N; 500/well plated as 2-day old organoids) and treated with a 10-point titration of cisplatin. PDOs were stained with Hoechst as the gold standard reference method and used for validation of BF image analysis. Despite varying levels of cytotoxicity from the chemotherapeutic treatment, the data showed that organoids were successfully identified from BF images (Fig. S2). Importantly, common artefacts (e.g. air-bubbles, extracellular matrix, dust) did not disrupt BF analysis (Fig. S2).

To further develop the applicability of the OrBITS platform, we investigated the capacity for intra-well normalization of organoid death with cell death markers, such as Cytotox Green. Since Hoechst and Cytotox Green are both nuclear stains, the overlap of Green Area or Green Intensity (RFU) with Hoechst allowed for intra-well normalization to study varying levels of cell death from the chemotherapeutic treatment (Fig. 3A). Importantly, pairwise comparison showed a strong correlation between BF and Hoechst normalized Green Area and Green Intensity, thus making a fluorescent viability stain (nuclear or cytoplasmatic) redundant (Fig. 3B). Total Green Area / Total Mask Area resulted in the broadest dynamic range (~Δ0.6 vs. ~Δ0.4), although a complete overlap ($R = 1$) in the 100 % cell death control (100 µM CDDP) was not reached (Fig. 3B). Therefore, the proposed platform provides an important advantage by including intra-well, normalized organoid death, even without the use of a viability label.

Overall, we showed that our OrBITS platform can mask organoids with high accuracy ranging from single cells to full-grown organoids based on BF imaging. In addition, inclusion of a

fluorescent cell death marker allowed for kinetic detection of intra-well normalized organoid death. This allows for the removal of a nuclear or cytoplasmatic viability stain during kinetic analysis, a key limitation of the current state-of-the-art analysis, as it can influence cellular growth and health and confounds the effect of treatments.

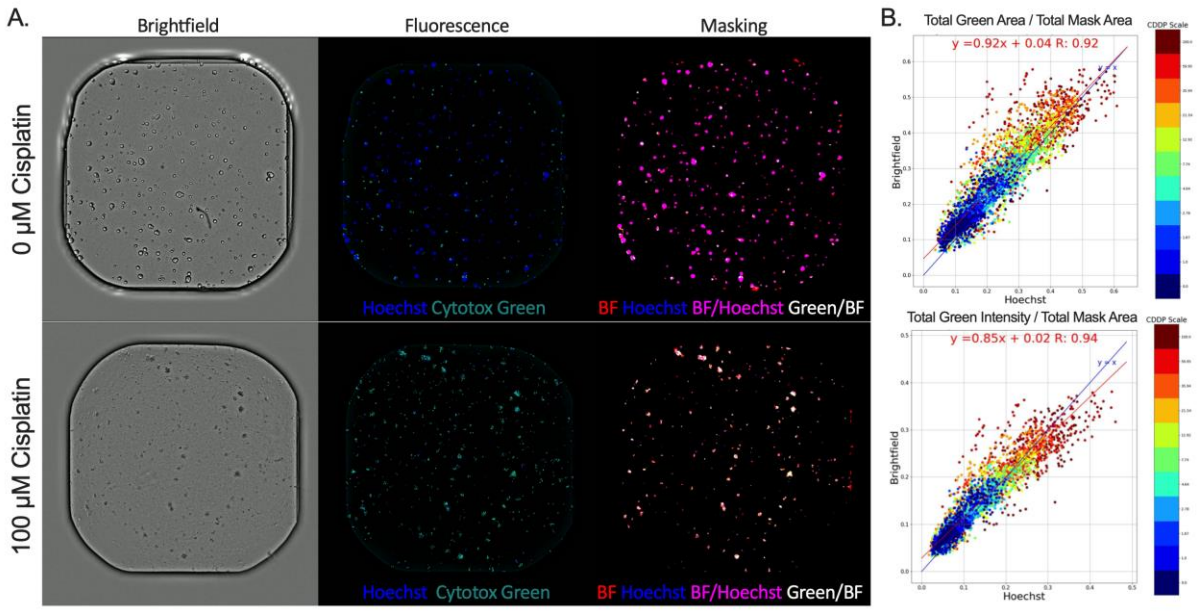

Figure 3: Brightfield vs Hoechst normalized fluorescent cell death marker. (A) Representative brightfield and fluorescent (Hoechst and Cytotox Green) images of untreated and 100 µM cisplatin (CDDP) treated NSCLC_051T PDOs and the corresponding masking of Brightfield, Hoechst, Brightfield/Hoechst overlap and Cytotox Green/Brightfield overlap. (B) Pairwise comparison of Total Green Area / Total Mask Area (per well: $\mu m^2/ \mu m^2$) and Total Green Intensity / Total Mask Area (per well: RFU/ μm^2) with Mask Area based on either Hoechst fluorescence imaging or BF imaging (Table S2).

Validation of OrBITS brightfield PDO monitoring in proof-of-concept drug screening: Comparison to CellTiter-Glo3D

In order to determine the if the OrBITS platform could accurately monitor viability and therapy response in PDOs, we compared the BF image analysis with the current industry and research standard: CellTiter-Glo 3D viability assay. PDOs were again treated with a 10-point titration of cisplatin, analyzed with both the OrBITS platform and the CellTiter-Glo 3D viability assay, and

the read-outs were compared. Pairwise comparison revealed that the Total Mask Area had the strongest correlation with the CellTiter-Glo 3D luminescent signal, since both parameters result from whole-well readouts (Fig. 4A).

The assay quality was assessed based on the Z-factor, a coefficient reflective of both assay signal dynamic range and data variation, using 100 µM cisplatin as positive control for NSCLC_051T. The CellTiter-Glo 3D read-out was characterized by a Z-factor of 0.78 and the Total BF Area by a Z-factor of 0.69, indicating that the BF assay is excellent for drug screening. When applying both vehicle (100% viability; PBS) and baseline normalization (0% viability; 100 µM cisplatin) no significant difference was observed between IC50 values obtained by the Total BF Area analysis and CellTiter-Glo 3D assay (Fig. 4B).

To validate our approach, we performed a drug screen of 6 standard-of-care lung cancer treatments on an additional PDO line (NSCLC_013T) using 1 µM staurosporine as the standardized 100% cell death control. A clear overlap of the inhibitory dose-response curves (Fig. 4C) and corresponding IC50 values (Fig. S3) was observed between the Total Mask Area analysis and CellTiter-Glo 3D assay. Therefore, it was clear that the OrBITS platform could accurately monitor PDOs for various anti-cancer drug screenings.

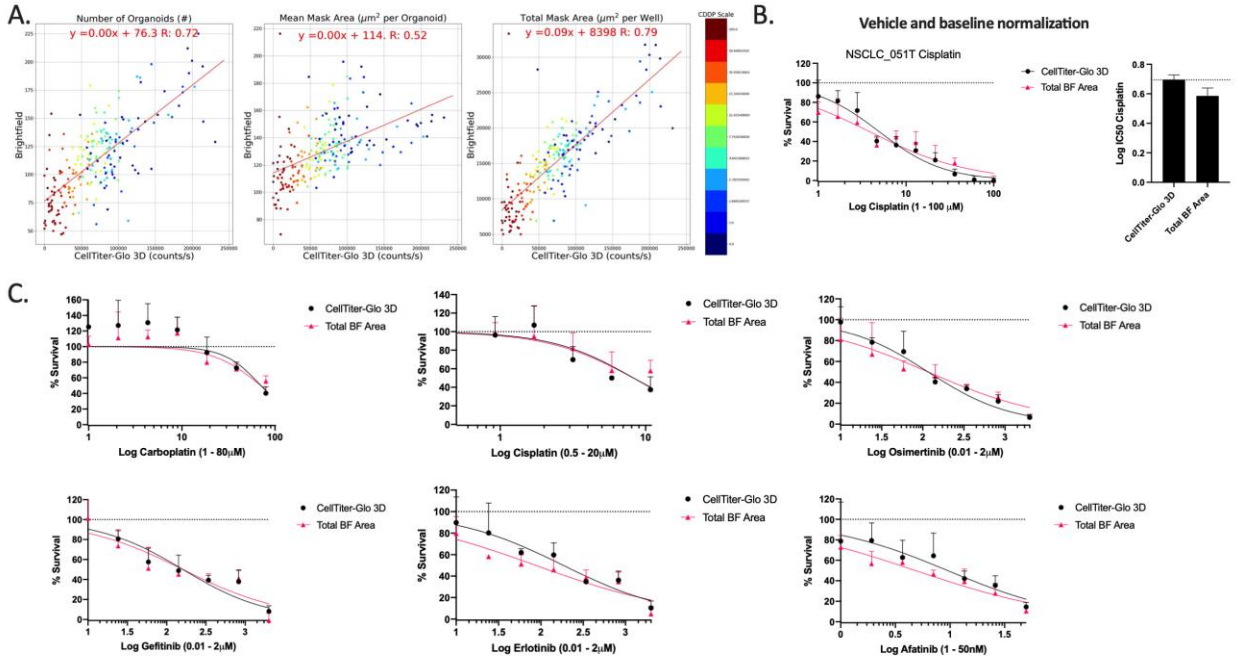

Figure 4: Brightfield imaging as a viability marker to monitor therapy response. (A) Pairwise comparison of organoid Count, Mean Mask Area and Total Mask Area with the luminescent read-out (counts/s) of the CellTiter-Glo 3D assay for the NSCLC_051T, NSCLC_051N, co-culture NSCLC_051T/N and NSCLC_050N PDO lines treated with a 10-point titration of cisplatin. Both read-outs were acquired at the same timepoint (114 hours) (Table S2). (B) Dose-response curve and corresponding IC50-values for NSCLC_051T treated with a 10-point titration of cisplatin and normalized to vehicle (100%) and baseline (0%, 100 µM cisplatin). (C) Dose-response curves of NSCLC_013T PDOs treated with a 7-point titration of cisplatin, carboplatin, erlotinib, gefitinib, osimertinib or afatinib normalized to vehicle (100%) and baseline (0%, 1 µM staurosporine). Corresponding IC50 values are presented in fig. S3. Graphs presented as mean ± SD of 5 technical replicates.

We observed that the Total BF Area resulted in an overestimation of the percentage of viable cells compared to the CellTiter-Glo 3D assay, following normalization to the vehicle control (Fig. 5A-C). The difference increased with cisplatin concentration, which was not unexpected since dead organoids were still counted by BF imaging. Therefore, we used a fluorescent cell death marker (Cytotox Green or equivalent) to correct for the area covered by dead entities, thus producing the parameter Total BF Area – Total Green Area. This parameter was characterized by a Z-factor of 0.80 for the NSCLC_051T line and both the dose-response curves and IC50-values showed an improved overlap with the CellTiter-Glo 3D assay for NSCLC_051T, 051N/T and 051N organoids

(Fig. 5A-C). Importantly, the parameter showed a clear distinction in sensitivity between the NSCLC_051T and NSCLC_051N lines, with an intermediate response in the co-culture of both lines (Fig. 5D). In addition, this parameter allowed for kinetic monitoring of cell viability (Fig. 5E) and vehicle-normalized survival (Fig. 5F), thus making early detection of therapy response possible.

Overall, we demonstrated that the parameters used in our proposed BF image analysis were robust and determined cell viability and IC50-values corresponding to the gold standard CellTiter-Glo 3D assay. Our OrBITS platform is a significant advance from the current gold standard assay by addressing its intrinsic limitations, as it allows for kinetic monitoring of organoid health and growth from limited starting material and independent of metabolic changes.

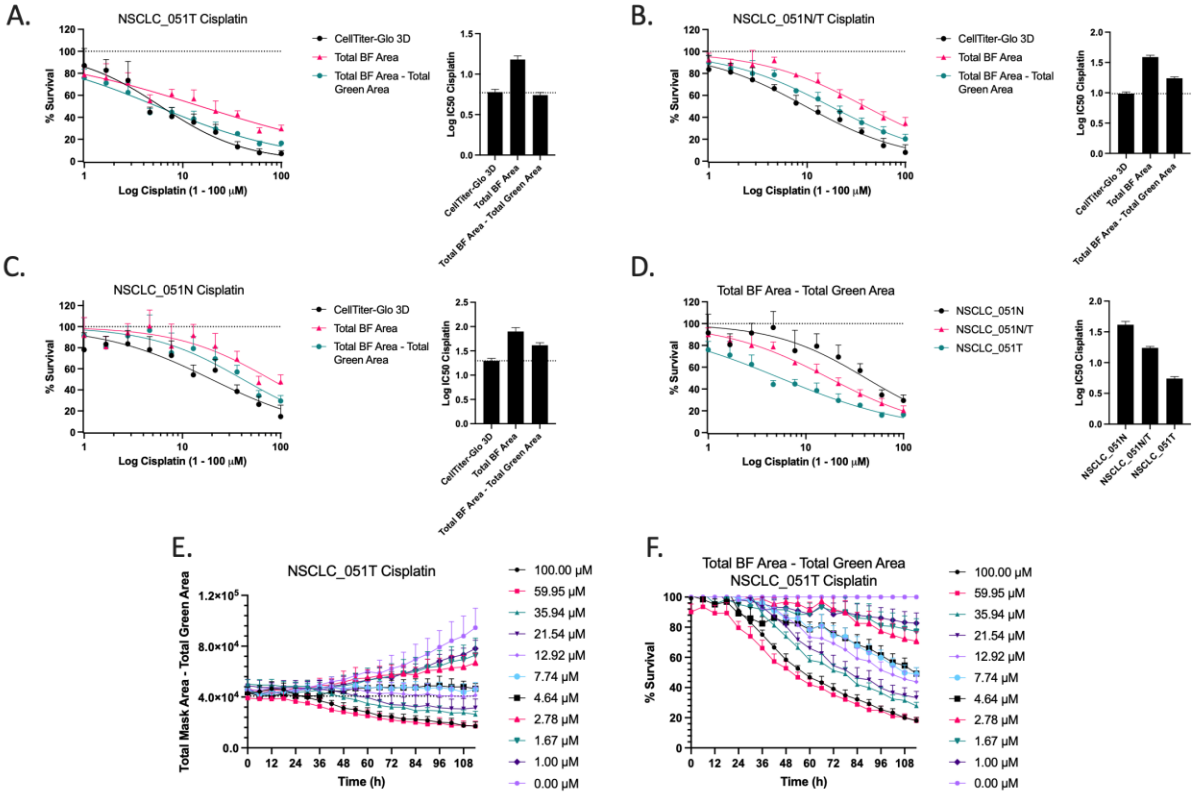

Figure 5: Cell death corrected vehicle normalization. (A-C) Dose-response curves and corresponding IC50-values for NSCLC_051T, NSCLC_051N and co-culture NSCLC_051N/T treated with a 10-point titration of cisplatin and normalized to vehicle (100%) control. Real-time monitoring of (E) cell viability and (F) survival percentage of NSCLC_051T PDOs treated with a 10-point titration of cisplatin. Percent survival was baseline corrected to vehicle control at each timepoint. Graphs presented as mean ± SD of 5 technical replicates.

Validation of OrBITS analysis to delineate cytostatic and cytotoxic anti-cancer therapy response

The ATP-based PDO drug screening analysis method does not provide insight into the mechanistic action of the drug, and therefore, we aimed to distinguish a cytostatic response (i.e. growth arrest) from a cytotoxic response (i.e. cell death) using the OrBITS platform. To achieve this, we quantified the amount of therapy-induced organoid death using our BF image analysis and the CellTiter-Glo 3D assay. Pairwise comparison showed an inverse correlation of Total Green Area and Total Green Intensity normalized to Total BF Area with the CellTiter-Glo 3D readout (Fig. 6A). The assay quality was assessed based on the Z-factor using 100 µM cisplatin as positive control for NSCLC_051T.Total Green Area / Total BF Area and Total Green Intensity / Total BF Area were characterized by a Z-factor of 0.71 and 0.75, respectively, consistent with a robust assay. A clear inverse relation was observed for the inhibitory dose-response curve (% survival) and stimulatory dose-response curve of both the Total Green Area and Intensity parameters normalized to BF area (% cell death) for cisplatin treated NSCLC_051T PDOs, suggesting a cytotoxic response in this organoid line (Fig. 6B). An example of a cytostatic response is given for NSCLC_013T treated with gefitinib (Fig. 6C). The use of Total Green Area was a more standardized parameter since it was less susceptible to variability compared to the Total Green Intensity parameter (e.g. led intensity, exposure time, and dye concentration). In addition to delineating cytotoxic and cytostatic therapy responses, our platform allowed for kinetic monitoring of therapy-induced cell death (Fig. 6D) and assessment of organoid health (growth and viability) as an imperative run quality control (Fig. 6E). Moreover, our platform allowed for more in-depth

research on the type of therapy-induced cell death that occurred. For example, cisplatin induced caspase 3/7 activity in NSCLC_046T, which is partly inhibited by the pan-caspase inhibitor Z-VAD-FMK (Fig. 6F). Consistently, Z-VAD-FMK inhibited cisplatin induced cell death, indicating that cytotoxicity occurs through caspase-dependent apoptosis (Fig. 6G). Here, the importance of kinetic monitoring is further highlighted, as the inhibitory effect of Z-VAD-FMK is nullified at 72h.

Overall, we demonstrated that the OrBITS platform allowed for kinetic and endpoint analysis of therapy-induced cell death to distinguish cytostatic from cytotoxic responses and can be further developed to provide in-depth insight into the mechanistic action.

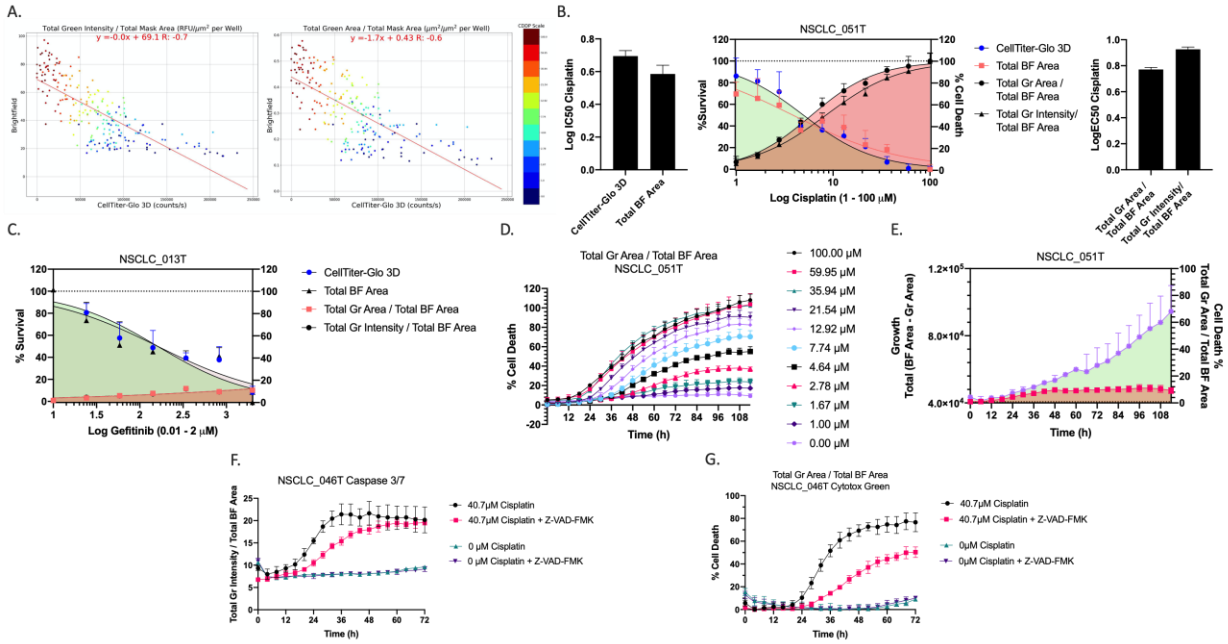

Figure 6: Fluorescent/brightfield imaging as a cell death marker. (A) Pairwise comparison of Total Green Intensity and Total Green Area (Cytotox Green reagent) normalized to Total BF Area with the luminescent read-out (counts/s) of the CellTiter-Glo 3D assay for the NSCLC_051T, NSCLC_051N, co-culture NSCLC_051T/N and NSCLC_050N PDO lines treated with a 10-point titration of cisplatin (Table S2). (B) Inhibitory (% survival, normalized to vehicle (100%) and baseline control (0%, 100 µM cisplatin) and stimulatory (% cell death, normalized to vehicle (0%) and positive control (100% , 100 µM cisplatin) dose-response curves and the corresponding IC50 and EC50 values for NSCLC_051T PDOs treated with a 10-point titration of cisplatin. (C) Inhibitory (% survival, normalized to vehicle (100%) and baseline control (0%, 1 µM staurosporine) and stimulatory (% cell death,

normalized to vehicle (0%) and positive control (100% , 1 µM staurosporine) dose-response curves NSCLC_013T PDOs treated with a 7-point titration of gefitinib. (D) Real-time monitoring of therapy-induced cell death of NSCLC_051T PDOs treated with a 10-point titration of cisplatin. Total Green Area / Total BF Area was normalized to baseline (0%, vehicle at t = 0h) and positive (100%, 100 µM cisplatin at t = 72h) controls. (E) Real-time monitoring of organoid growth (Total BF Area – Total Green Area) and cell death (Total Green Area / Total BF Area) as run quality control. (F) Total Green Intensity / Total BF Area of the Caspase 3/7 green reagent in NSCLC_046T PDOs treated with cisplatin +/- Z-VAD-FMK (pan-caspase inhibitor). (G) Percentage of cell death of NSCLC_046T organoids treated with cisplatin +/- Z-VAD-FMK. Total Green Area / Total BF Area was normalized to baseline (0%, lowest value) and positive (100%, 75 µM cisplatin at t = 72h) controls. Graphs presented as mean ± SD of 5 technical replicates.

Broad applicability of OrBITS for various organoid platforms and cancer cell lines

While the OrBITS platform was developed using lung organoids in a high-throughput 384-well plate format, we have also successfully implemented the image analysis method for a range of cancer cell lines and PDOs of other tumor types. For example, we demonstrated the precise tracking capability on the growth of 3 cell lines (NCI-H1975, HCT-15, and NCI-H460) and pancreatic cancer-derived organoids, using BF imaging (Supplemental Video 4). Furthermore, we showed that OrBITS was able to accurately mask pancreatic cancer organoids embedded in extracellular matrix domes, which further allows monitoring of routine organoid cultures in various culture plates and long-term screening assays (Fig. 7A, Supplemental Video 5). Lastly, OrBITS BF image analysis was tested on the Gri3D®-96 well plates, a novel organoid plate format with hydrogel-based microcavities for high-throughput organoid cultures[14]. Impressively, OrBITS accurately discriminated organoids from background in the BF images without additional training of the convolutional neural network (Fig. 7B, Supplemental Video 6). Overall, we showed that the OrBITS platform has broad applicability, in terms of various cell and organoid types, as well as culturing methods, ranging from conventional to state-of-the art.

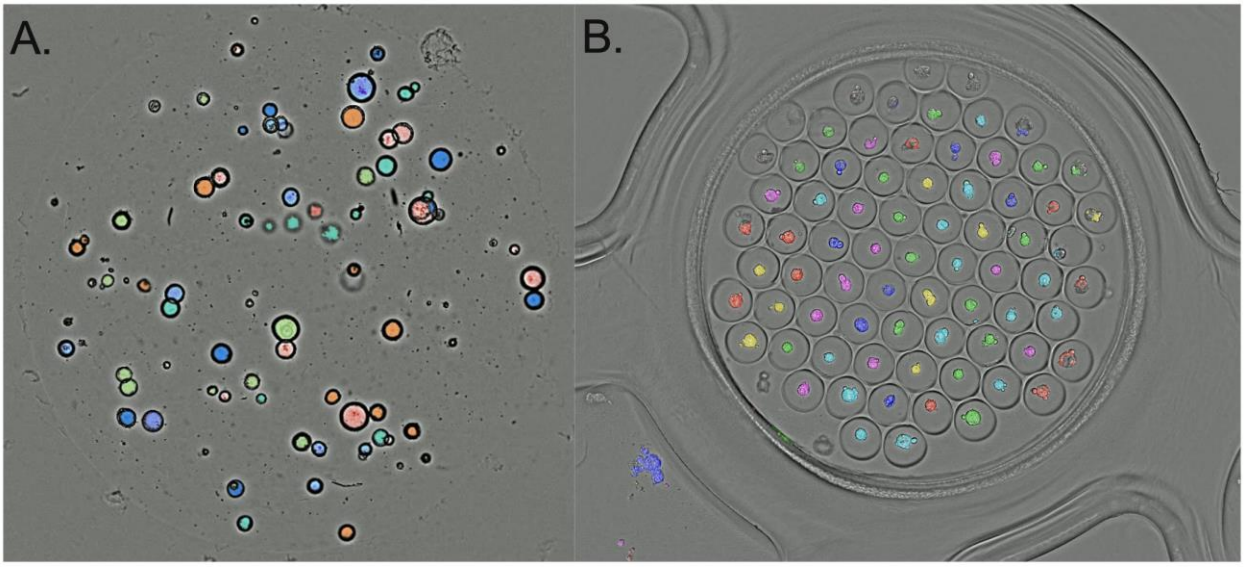

Figure 7: Examples of the broad applicability of OrBITS. (A) Cystic pancreatic cancer organoids grown in an extracellular matrix dome. Kinetic growth monitoring is shown in supplemental video 5. **(B)** Cancer cell line spheroids grown in a Gri3D®-96 well plate. Kinetic growth monitoring is shown in supplemental video 6.

Discussion

In this study we validated a new brightfield imaging-based method for ex vivo drug screening on patient-derived organoids. The Spark Cyto 600 system used here is a state-of-the art multimode plate reader with BF and fluorescence imaging capabilities. With full environmental controls (e.g. O_2, CO_2, temperature) and an injector, we automated the system to plate single cells or full-grown organoids, perform kinetic measurements, and dispense reagents (e.g. CellTiterGlo-3D) for endpoint analysis. This greatly improves the organoid culture by reducing variability involved with the cumbersome manual cultures, particularly in 384-well plates. While this all-in-one system ideal for the clinical implementation of drug sensitivity screens on patient-derived tumor organoids, the current limitation is the Image Analyzer software, which is limited to 2D analysis. Therefore, we developed a deep learning solution for 3D organoid/spheroid segmentation based on BF images

acquired with the Spark Cyto. Altogether, these features make up our OrBITS platform which provides, an advanced high-throughput, time-lapse drug screening platform.

Our system identifies organoids from BF images, thus removing the need for nuclear labeling, which can affect biological process and confound therapy responses. As demonstrated, there are several benefits to using the BF channel to detect and measure organoids over transient or stably expressed fluorescent markers. These include: (i) the ability to detect organoids in cases where high cell death reduces detectability via nuclear markers; (ii) increased reproducibility since variance related to dye concentrations, stability (e.g. photobleaching), LED intensity, and exposure time is removed; (iii) the ability to detect cystic organoids, which can be problematic since Hoechst only stains the outer edge of cystic organoids; (iv) optimal size and growth metrics, since it is not guaranteed that all parts of the cellular structure will contain viable nucleated cells as organoids grow, and therefore, reliance of fluorescent markers therefore must be limited; (v) the ability to distinguish valid organoids from artifacts such as cellular debris which may produce false positives or bubbles which may occlude cells; (vi) and lastly, the reduction of any interfering effects of repeated fluorescence imaging on growth and metabolism due to the release of reactive oxygen species by photoexcited fluorophores and other side-effects related to phototoxicity[15].

Without the need to consider cytotoxic interference, imaging can be performed at higher frequency time intervals. This opens up new possibilities for studies into how drugs affect organoid growth and migration over time, which is currently not possible with simple endpoint assays. A key measurement parameter of drug screening studies is cell viability. This is commonly done using CellTiter-Glo 3D which, as an endpoint assay, is highly constrained. Alternatives to CellTiter-Glo 3D for measurement of cell death and viability are especially welcomed, since several therapies

are known to affect the primary parameter of measurement for CellTiter-Glo 3D (ATP) via modulating intracellular ATP levels or releasing extracellular ATP following (immunogenic) cell death[16]. Furthermore, this approach does not distinguish cytotoxic from cytostatic responses, which could further improve translatability of drug responses to the clinic and requires further investigation.

Using the OrBITS platform, we demonstrated that organoid can be grown from either single-cells or full-grown organoids with equal efficiency in 384-well plates. Gao et. al recently demonstrated that organoids starting from single-cells demonstrated similar sensitivity to cytotoxic drugs to matched full grown organoids [17]. Therefore, our platform can greatly reduce turn-around time for *ex vivo* drug screenings as OrBITs can accurately monitoring organoid growth, health and therapy response with a limited amount of starting material. In addition, kinetic imaging allows for early detection of therapy response and the use of growth rate metrics has been shown to result in higher reproducibility via uncoupling the effect of cell proliferation on drug sensitivity [18,19].

Here, we demonstrated organoid identification, growth, and death using BF images, but we have only begun to tap into the potential of BF image analysis. In principle, other morphological changes with clinical and research implications are currently being pursued for organoids, 3D spheroid cultures, and 2D monolayers. We also demonstrated the flexibility of the OrBITS platform to differing culture methods ranging from conventional (e.g. well-plates, matrix domes) to state-of-the-art (Gri3D®-96). Furthermore, we demonstrate the analysis capability on various cell and organoids lines apart from those used for developing the BF imaging software. In the process, we confirmed the challenges related to establishing lung cancer organoids as described by Dijkstra et al.[13]. A more minimal medium compared to the one used in this study has recently

been described which should limit the growth of normal lung organoids [22], although we observed no sustained organoid growth tested in a small set of samples. The use of Napsin A, p63 or p40 (ΔNp63) and TTF-1 allows for identifying cultures overgrown by non-malignant lung cells. As such, the patient-derived organoids used in our method development were non-malignant organoids displaying either a solid (derived from tumor tissue) or cystic (derived from healthy tissue) growth pattern. Apart from the clear difference in morphology, the non-malignant organoids derived from tumor tissue (NSCLC_051T) were more sensitive to cisplatin compared to the organoids derived from healthy tissue from the same patient (NSCLC_051N). This further indicates that these cells have different characteristics which could influence the outcome of a drug sensitivity screen if present in tumor organoid cultures. Even so, our method will also be applicable in tumor organoids since they present a similar growth pattern [13,22].

Methods

Patient tissue

Tumor tissue and normal lung tissue (distant from the tumor site) were obtained from adeno- and squamous cell carcinoma NSCLC patients undergoing curative surgery at the Antwerp University Hospital (UZA) in 2019-2020. Written informed consent was obtained from all patients, and the study was approved by the UZA Ethical Committee (ref. 17/30/339). All samples were registered in the Biobank Antwerp, Belgium; ID: BE 71030031000.

Tissue processing and organoid culture

Tissue was stored in Ad-DF+++ (Advanced DMEM/F12 (GIBCO), with 1% GlutaMAX (GIBCO), 1% HEPES (GIBCO), 1% penicillin/streptomycin (GIBCO) supplemented with 2% Primocin (Invivogen) at 4°C and transported on ice to be processed within 24 hours for organoid culture according to the protocol of Dijkstra et al. [13] with some minor differences. Tumor and normal tissue were minced with two scalpels, collected in 0.1% BSA precoated tubes and washed with PBS. Next, fragments were dissociated with 0.5 mg/mL dispase type II (Sigma-Aldrich), 1.5 mg/mL collagenase type II (Sigma-Aldrich), 1:500 Primocin and 10 µM Y-27632 (Cayman Chemicals) in MG^{2+}/Ca^{2+} PBS (GIBCO) for 60 minutes at 37°C. Digested cells were washed three times with PBS and resuspended in 2/3 Cultrex Type 2 (R&D Systems) and 1/3 Full Lung Ad-DF+++ medium and plated in drops which were allowed to solidify for 30 minutes at 37°C after which they were overlayed with Full Ad-DF+++ medium. Full Ad-DF+++ medium consisted of 10% Noggin conditioned medium (HEK293-mNoggin-Fc; kindly provided by Hans Clever, Hubrecht Institute), 10% R-spondin-1 conditioned medium (293T-HA-Rspol-Fc; kindly provided by Calvin Kuo, Stanford University), 1 x B27 supplement (GIBCO), 10 mM nicotinamide (Sigma-

Aldrich), 25 ng/mM human recombinant FGF-7 (Peprotech), 100 ng/mL human recombinant FGF-10 (Peprotech), 500 nM A83-01 (Tocris), 1 µM SB202190 (Cayman Chemicals) and 5 µM Y-27632 (only used after passaging and thawing). For passaging, organoids were digested to single cells with TrypLE Express (GIBCO). For cryopreservation, 3-day old organoids were harvested with Cultrex Harvesting Solution (R&D Systems) and frozen in Recovery Cell Culture Freezing Medium (GIBCO). Samples were tested for Mycoplasma contamination with the MycoAlert Mycoplasma Detection Kit (LONZA).

Immunohistochemical analysis

Early passage organoids were collected using Cultrex Organoid Harvesting Solution (R&D systems), washed with ice-cold PBS, and fixated in 4% paraformaldehyde for 30 minutes at room temperature. Fixed organoids were transferred to a 4% agarose micro-array mold and paraffin-embedded as described before [23]. Five µm-thick sections were prepared, deparaffinized and rehydrated prior to staining. Sections were subjected to heat-induced antigen retrieval by incubation in a low pH buffer (Envision Flex TRS low pH (DAKO) for 20 min at 97°C (PT-Link, DAKO). Endogenous peroxidase activity was quenched by incubation in peroxidase blocking buffer (DAKO) for 5 min. Slides were stained manually with mouse anti-TTF1 (clone SPT24, Leica, 1/400, 25') and mouse anti-P40 (clone BC28, Biocare, ready-to-use, 30') primary antibodies followed by an incubation with ENVISION Flex+ Mouse Linker (DAKO, 15') for signal amplification. Mouse anti-NapsinA (clone MRQ-60, Cell Marque, 1/350, 35') staining was performed on a DAKO autostainer Link 48. After that the slides were incubated for 25 min with Envision FLEX/HRP (ready-to-use, DAKO) secondary antibody followed by 10 min incubation with the DAB substrate/chromogen detection system (DAKO). The sections were counterstained

for 2 min with hematoxylin (0.1%), dehydrated and mounted with Quick-D Mounting Medium (KliniPath). Sections were imaged using a Leica DM500 microscope equipped with an ICC50 E camera.

In vitro drug screen

Three days before the start of the experiment, organoids were passaged as single cells using TrypLE and plated in Cultrex drops. Subsequently, organoids were harvested with Cultrex Harvesting Solution, collected in 15 mL tubes coated with 0.1% BSA/PBS, washed with Ad-DF+++ and resuspended in 1 mL Full Ad-DF+++ medium (without Y-27632). Next the number of organoids were counted with the Sceptor 2.0 using a 60 µM sensor (Merck Millipore). Organoids were then diluted in Full Ad-DF+++ and 5% Cultrex on ice to a concentration that results in 500-2000 organoids/60µL. 60µL of this solution was plated into a 384-well ultra-low attachment microplate (Corning, #4588) using the Tecan Spark Cyto Injector at a speed of 100 µL/s to avoid bubbles. All tubes and the Spark Cyto Injector were primed with 0.1 % BSA/PBS to avoid sticking of the organoids. Next, the plate was centrifuged (100 rcf, 30 sec, 4°C) and incubated for at least 30 minutes at 37°C.

All drugs and fluorescent reagents were added to the plate using the Tecan D300e Digital Dispenser. Cytotox Green (75 nM / well, Sartorius), Caspase 3/7 Green Reagent (2.5 µM / well, Sartorius), Z-VAD-FMK (50 µM / well, Bachem AG), Erlotinib, Gefitinib, Osimertinib and Afatinib (Selleckchem) were dissolved in DMSO. Hoechst 33342 (50 nM / well, ThermoFisher), Cisplatin (Tocris) and Carboplatin (Selleckchem) were dissolved in PBS to yield a final concentration of 0.3 Tween-20 required for dispensing with the D300e Dispenser.

BF, green and blue fluorescence whole-well images (4x objective) were taken with the Tecan Spark Cyto set at 37°C / 5% CO_2 for kinetic experiments in a humidity cassette. For endpoint measurement of ATP levels, 60 µL CellTiter-Glo 3D reagent (Promega) was injected using the Tecan Spark Cyto Injector to each well, shaken for 5 minutes and measured after 30 minutes incubation with the Tecan Spark Cyto luminescence module.

Dose-response curves plotted, and IC_{50}-values were calculated using GraphPad Prism 9. Drug concentrations were transformed to log10 and raw data results were normalized to vehicle (100%) and/or baseline control (0%) (Staurosporin 5 µM or 100 µM cisplatin) for viability assessment, and vice versa for cell death assessment. Curves were fitted using the log (inhibitor/agonist) vs. normalized response - Variable slope function. Screen quality was determined by calculating the Z Factor score using the formula [24]:

$$1 - \frac{3 * SD\ (negative\ control) + 3 * SD\ (positive\ control)}{average\ (negatrive\ control) - average\ (positive\ control)}$$

Image-based analysis

Following image acquisition with the Tecan Spark Cyto, BF and fluorescence images were analyzed by the University of Antwerp Service Platform: OrBITS Platform. The analysis output from OrBITS (Table S1) was correlated with the current gold standard assays: Hoechst staining (for organoid tracking), Cytotox Green (for organoid death), and the CellTiter-Glo 3D assay (for drug screening).

Acknowledgements

This work was funded in part by the Flanders Research Foundation, 12S9221N (A.L.), 12S9218N (A.L.), G044420N (A.B., S.V., A.L.) and by the Industrial Research Fund of the

University of Antwerp, PS ID 45151 (C.D., S.V., A.L.). We would like to thank Mr. Willy Floren for funding the D300e and Tecan for gifting the Spark Cyto as part of a competition.

Authors contribution

C.D, E.C.DLH. and A.L. conceived the idea and wrote the manuscript. C.D., M.L.C. performed the in vitro experiments. E.C.DLH. developed the software and analyzed the data. P.V.S., J.M.H, P.L, S.K.Y supplied the patient derived materials. F.L, P.P, A.B, E.S., A.L. substantially revised the manuscript.

Competing interests

The authors declare no competing interests.

References

1 Drost, J. & Clevers, H. Organoids in cancer research. *Nat Rev Cancer* **18**, 407-418, doi:10.1038/s41568-018-0007-6 (2018).

2 Narasimhan, V. *et al.* Medium-throughput Drug Screening of Patient-derived Organoids from Colorectal Peritoneal Metastases to Direct Personalized Therapy. *Clinical cancer research : an official journal of the American Association for Cancer Research*, doi:10.1158/1078-0432.CCR-20-0073 (2020).

3 Ooft, S. N. *et al.* Patient-derived organoids can predict response to chemotherapy in metastatic colorectal cancer patients. *Science translational medicine* **11**, doi:10.1126/scitranslmed.aay2574 (2019).

4 Driehuis, E. *et al.* Pancreatic cancer organoids recapitulate disease and allow personalized drug screening. *Proceedings of the National Academy of Sciences of the United States of America*, doi:10.1073/pnas.1911273116 (2019).

5 Driehuis, E. *et al.* Patient-Derived Head and Neck Cancer Organoids Recapitulate EGFR Expression Levels of Respective Tissues and Are Responsive to EGFR-Targeted Photodynamic Therapy. *J Clin Med* **8**, doi:10.3390/jcm8111880 (2019).

6 Driehuis, E. *et al.* Oral Mucosal Organoids as a Potential Platform for Personalized Cancer Therapy. *Cancer discovery* **9**, 852-871, doi:10.1158/2159-8290.Cd-18-1522 (2019).

7 Vlachogiannis, G. *et al.* Patient-derived organoids model treatment response of metastatic gastrointestinal cancers. *Science* **359**, 920-926, doi:10.1126/science.aao2774 (2018).

8 Nagle, P. W., Plukker, J. T. M., Muijs, C. T., van Luijk, P. & Coppes, R. P. Patient-derived tumor organoids for prediction of cancer treatment response. *Seminars in cancer biology* **53**, 258-264, doi:10.1016/j.semcancer.2018.06.005 (2018).

9 Choi, Y. M. *et al.* Mechanism of Cisplatin-Induced Cytotoxicity Is Correlated to Impaired Metabolism Due to Mitochondrial ROS Generation. *PloS one* **10**, e0135083, doi:10.1371/journal.pone.0135083 (2015).

10 Shirmanova, M. V. *et al.* Chemotherapy with cisplatin: insights into intracellular pH and metabolic landscape of cancer cells in vitro and in vivo. *Sci Rep* **7**, 8911, doi:10.1038/s41598-017-09426-4 (2017).

11 Zhou, Y. *et al.* Intracellular ATP levels are a pivotal determinant of chemoresistance in colon cancer cells. *Cancer research* **72**, 304-314, doi:10.1158/0008-5472.Can-11-1674 (2012).

12 Turner, B. M. *et al.* Napsin A, a new marker for lung adenocarcinoma, is complementary and more sensitive and specific than thyroid transcription factor 1 in the differential diagnosis of primary pulmonary carcinoma: evaluation of 1674 cases by tissue microarray. *Arch Pathol Lab Med* **136**, 163-171, doi:10.5858/arpa.2011-0320-OA (2012).

13 Dijkstra, K. K. *et al.* Challenges in Establishing Pure Lung Cancer Organoids Limit Their Utility for Personalized Medicine. *Cell Rep* **31**, 107588, doi:10.1016/j.celrep.2020.107588 (2020).

14 Brandenberg, N. *et al.* High-throughput automated organoid culture via stem-cell aggregation in microcavity arrays. *Nat Biomed Eng* **4**, 863-874, doi:10.1038/s41551-020-0565-2 (2020).

15 Icha, J., Weber, M., Waters, J. C. & Norden, C. Phototoxicity in live fluorescence microscopy, and how to avoid it. *Bioessays* **39**, doi:10.1002/bies.201700003 (2017).

16 Krysko, D. V. *et al.* Immunogenic cell death and DAMPs in cancer therapy. *Nat Rev Cancer* **12**, 860-875, doi:10.1038/nrc3380 (2012).

17 Gao, M. *et al.* Development of a Single-Cell Technique to Increase Yield and Use of Gastrointestinal Cancer Organoids for Personalized Medicine Application. *J Am Coll Surg*, doi:10.1016/j.jamcollsurg.2020.11.009 (2020).

18 Driehuis, E., Kretzschmar, K. & Clevers, H. Establishment of patient-derived cancer organoids for drug-screening applications. *Nat Protoc* **15**, 3380-3409, doi:10.1038/s41596-020-0379-4 (2020).

19 Hafner, M., Niepel, M., Chung, M. & Sorger, P. K. Growth rate inhibition metrics correct for confounders in measuring sensitivity to cancer drugs. *Nat Methods* **13**, 521-527, doi:10.1038/nmeth.3853 (2016).

20 Baker, L. A., Tiriac, H. & Tuveson, D. A. Generation and Culture of Human Pancreatic Ductal Adenocarcinoma Organoids from Resected Tumor Specimens. *Methods in molecular biology* **1882**, 97-115, doi:10.1007/978-1-4939-8879-2_9 (2019).

21 Kassis, T., Hernandez-Gordillo, V., Langer, R. & Griffith, L. G. OrgaQuant: Human Intestinal Organoid Localization and Quantification Using Deep Convolutional Neural Networks. *Sci Rep* **9**, 12479, doi:10.1038/s41598-019-48874-y (2019).

22 Kim, M. *et al.* Patient-derived lung cancer organoids as in vitro cancer models for therapeutic screening. *Nature communications* **10**, 3991, doi:10.1038/s41467-019-11867-6 (2019).

23 Ivanov, D. P. & Grabowska, A. M. Spheroid arrays for high-throughput single-cell analysis of spatial patterns and biomarker expression in 3D. *Sci Rep* **7**, 41160, doi:10.1038/srep41160 (2017).

24 Zhang, J. H., Chung, T. D. & Oldenburg, K. R. A Simple Statistical Parameter for Use in Evaluation and Validation of High Throughput Screening Assays. *J Biomol Screen* **4**, 67-73, doi:10.1177/108705719900400206 (1999).